Icarus 226 (2013) 898–904

Contents lists available at SciVerse ScienceDirect

Icarus

journal homepage: www.elsevier.com/locate/icarus

Impact of tidal heating on the onset of convection in Enceladus's ice shell

Marie Běhounková [a,*], Gabriel Tobie [b,c], Gaël Choblet [b,c], Ondřej Čadek [a]

[a] Charles University in Prague, Faculty of Mathematics and Physics, Department of Geophysics, V Holešovičkách 2, 180 00 Praha 8, Czech Republic
[b] Université de Nantes, LPGNantes, UMR 6112, F-44322 Nantes, France
[c] CNRS, LPGNantes, UMR 6112, F-44322 Nantes, France

ARTICLE INFO

Article history:
Received 12 February 2013
Revised 1 June 2013
Accepted 25 June 2013
Available online 18 July 2013

Keywords:
Enceladus
Ices
Tides, Solid body
Interiors
Thermal histories

ABSTRACT

By performing 3D simulations of thermal convection and tidal dissipation, we investigated the effect of tidal heating on the onset of convection in Enceladus's ice shell. We considered a composite non-Newtonian rheology including diffusion, grain-size-sensitive and dislocation creeps, and we defined an effective tidal viscosity reproducing the dissipation function as predicted by the Andrade rheology. For simulations with no or moderate tidal heating, the onset of convection requires ice grain sizes smaller than or equal to 0.5–0.6 mm. For simulations including significant tidal heating ($>10^{-6}$ W m^{-3}), the critical grain size for the onset of convection is shifted up to values of 1–1.5 mm. Whatever the width of the internal ocean, convection is initiated in the polar region due to enhanced tidal dissipation at high latitudes. For a given eccentricity value, the onset of convection depends on the ocean width, as tidal flexing and hence tidal heat production is controlled by the ocean width. For heating rates larger than 5–9 $\times 10^{-7}$ W m^{-3}, we systematically observe the occurrence of melting in our simulations, whatever the grain size and for both convecting and non-convecting cases. Grain sizes smaller than 1.5 mm, required to initiate convection, may be obtained either by the presence of a few percent of impurities limiting the grain growth by pinning effects or by the increase of stress and hence dynamic recrystallization associated with tidally-induced melting events.

1. Introduction

Observations of Enceladus by the Cassini spacecraft indicated that its south pole is very active, with jets of water vapor and ice emanating from warm tectonic ridges (Porco et al., 2006; Spencer et al., 2006, 2009). The heat power released from the south polar terrain was evaluated to be 15.8 ± 3.1 GW from the analysis of thermal emission spectra (Howett et al., 2011), which is much larger than what may be produced by decay of radioactive elements in the rocky core (Schubert et al., 2007). The abnormal endogenic power is most likely the consequence of strong tidal dissipation along the ridges and within the ice shell (Nimmo et al., 2007; Tobie et al., 2008). However, as tidal friction should result in a rapid damping of the orbital eccentricity, maintaining a highly dissipative state on geological timescales is challenging (Meyer and Wisdom, 2007; Zhang and Nimmo, 2009; Běhounková et al., 2012).

Convective processes in the ice shell are commonly advocated to induce the enhanced activity at the south pole (Nimmo and Pappalardo, 2006; Barr and McKinnon, 2007a; Mitri and Showman, 2008a,b; Roberts and Nimmo, 2008; Stegman et al., 2009; Běhounková et al., 2010; Han et al., 2012). The conditions under which convection may occur on Enceladus are, however, still puzzling. According to the estimation of Barr and McKinnon (2007a) based on scaling laws, convection may initiate in Enceladus's ice shell only for grain size smaller than 0.3 mm, which is very small compared the grain size observed on Earth in polar ice sheets for similar temperature and stress conditions (~2–4 mm, Durand et al. (2006)).

Moreover, for the present-day value of eccentricity, the power generated by tidal friction in the ice shell is modeled to be much smaller than heat loss by thermal convection (Roberts and Nimmo, 2008; Běhounková et al., 2012), suggesting that Enceladus may have experienced a recent period of enhanced eccentricity and dissipation. Using 3D simulations of thermal convection and tidal dissipation, we showed in our previous study (Běhounková et al., 2012) that periods with enhanced eccentricity can lead to tidally-induced melting events in the ice shell, potentially resulting in enhanced surface activities. However, we showed that such enhanced activity periods associated with thermal convection and internal melting should be brief (~1–10 Myr) followed by relatively long periods of inactivity (~100 Myr) during which the cessation of thermal convection is likely.

In order to constrain the duration and periodicity of enhanced thermal activity, we need to better understand the conditions

* Corresponding author.
E-mail addresses: marie.behounkova@mff.cuni.cz (M. Běhounková), gabriel.tobie@univ-nantes.fr (G. Tobie), gael.choblet@univ-nantes.fr (G. Choblet), oc@karel.troja.mff.cuni.cz (O. Čadek).

0019-1035/$ - see front matter © 2013 Elsevier Inc. All rights reserved.
http://dx.doi.org/10.1016/j.icarus.2013.06.033

under which thermal convection may initiate. In particular, our goal is to understand how tidal heating, especially during periods of elevated eccentricity, may influence the onset of convection. To answer this question, we performed 3D simulations of thermal convection including a self-consistent computation of tidal dissipation using the code ANTIGONE previously described in Běhounková et al. (2010, 2012). To better simulate the mechanical properties of the ice shell, we considered a composite non-Newtonian rheology including three creep mechanisms following Durham et al. (2001) and Goldsby and Kohlstedt (2001), and we defined an effective tidal viscosity reproducing the dissipation function of the Andrade model (Castillo-Rogez et al., 2011). Section 2 provides a brief description of the numerical model and describes the new implementation in addition to Běhounková et al. (2012). The onset of convection in a heterogeneously heated shell is discussed in Section 3. In Section 4, we present the simulation results for the onset of convection in a tidally-heated shell and determine the critical grain size under which convection may occur in Enceladus's ice shell as a function of tidal heating. Finally, in Section 5, we briefly discuss the implications of our results for the evolution of Enceladus.

2. Model and rheological description

In order to describe the onset of convection in a body undergoing strong tidal friction, we use a numerical tool described in Běhounková et al. (2010, 2012). This tool solves simultaneously the long-term viscous flow and the short-term viscoelastic response to a tidal forcing in a 3D spherical shell. Both processes are coupled via the viscosity field. For the viscous flow, the equations describing the mass, momentum and energy conservations are solved using the finite volume method ŒDIPUS (Choblet, 2005; Choblet et al., 2007). In the case of the viscoelastic response, the deformations (mass and momentum conservations) are solved in the time domain (Tobie et al., 2008). Owing to the different time scales of both processes, tidal deformation has no mechanical effect on convective motions, and therefore only the dissipative part is included as a heterogeneous source of volumetric heating in the energy equation for thermal convection.

2.1. Parameters and numerical procedure

In the present study, we concentrate on the onset of convection in a tidally-heated ice layer for different grain size values. As previously demonstrated in Běhounková et al. (2012), the amplitude and distribution of tidal dissipation are determined by the orbital eccentricity and the width of the internal water reservoir at the boundary between the ice layer and the rocky core. Following Běhounková et al. (2012), the presence of a deep water reservoir of finite lateral extent is included via the boundary conditions at the base of the ice layer. At the water/ice interface, a constant temperature corresponding to the melting point of pure water (273 K) is prescribed and a free-slip/force equilibrium mechanical condition is used. Outside the water region, a constant heat flux, q_b, and a no-slip mechanical condition are prescribed (see Běhounková et al., 2012 for more details). For simplicity, the deep water reservoir is assumed to be axisymmetric and centered at the south pole. Reservoir widths varying between 120° and 360° are considered. For reservoir widths smaller than 120°, no significant enhancement of tidal dissipation at the south pole is obtained (Tobie et al., 2008; Běhounková et al., 2012), and as we are mainly interested in the effect of large tidal heating on the onset of convection, configurations with a small liquid reservoir are not considered here.

Simulations are performed for fixed eccentricity values, varying between zero and five times the current value ($e_0 = 0.0045$). Simulations with no eccentricity/tidal heating are used as a reference to better highlight the influence of tidal dissipation. As illustrated in Běhounková et al. (2012), during periods of reduced dissipation, the orbital eccentricity may rapidly grow due to tidal dissipation in Saturn. Following the model of Meyer and Wisdom (2007), eccentricity values up to $5 \times e_0$ can be reached within few Myr for Saturn's quality factor, $Q_S = 1800$, and for a weakly dissipative interior of Enceladus (<1 GW). Although the orbital eccentricity is expected to vary on timescales of Myr, the value remains fixed in our simulation to better understand the role of enhanced tidal heating. Consistent time evolution of the orbital eccentricity will be considered in the future.

Our model includes a simple description of melting where any melt produced within the convective ice shell (once the temperature reaches the melting point) is instantaneously extracted downward to the underlying water reservoir. This simplification assumes that the melt extraction timescale is shorter than the convection timescale and that no residual melt remains in the ice matrix. Recent results of Kalousová et al. (2013) based on two-phase flow modeling of water–ice mixture show that water produced in tidally heated hot plumes is transported downwards very efficiently in the form of porosity waves, and that the melt fraction remains always below 1%. Although these results were obtained for Europa, they remain valid in Enceladus' conditions. Here, as no melt is considered in the matrix, no melt effect on the ice viscosity and density are included. The role of interstitial melt is further discussed in Section 5.

The physical parameters used are listed in Table 1. The initial conditions correspond to the conductive solution for the given width of the ocean, and they are initially perturbed with a maximum perturbation corresponding to 1% of the global temperature contrast. The discrete grid mesh is 6×64^3 for the computation of thermal convection. For the computation of the viscoelastic response, the same radial resolution (i.e. 64 layers) is used, and a spectral decomposition up to degree 80 in lateral directions is considered. For numerical reasons, a maximum viscosity contrast of 10^8 is considered within the computational domain in the case of thermal convection. When the computed viscosity exceeds $10^8 \times \eta_b$ (viscosity at the bottom of the ice shell), the viscosity is set to this cut-off value. The tidal deformation is recomputed every

Table 1
List of physical parameters used in this study.

Thermal conductivity[a]	k	2.3	W m^{-1} K^{-1}
Thermal expansivity[a]	α	1.6×10^{-4}	K^{-1}
Heat capacity[a]	c_p	2100	J kg^{-1} K^{-1}
Thermal diffusivity[a]	κ	1.19×10^{-6}	m^2 s^{-1}
Latent heat[a]	L	333	kJ kg^{-1}
Water ice density[a]	ρ_0	920	kg m^{-3}
Water density	ρ_w	1000	kg m^{-3}
Silicate core density	ρ_c	3000	kg m^{-3}
Reference gravity acceleration	g_0	0.113	m s^{-2}
Outer radius of the ice shell	r_t	252.3	km
Inner radius of the ice shell	r_b	169.5	km
Heat flux on bottom boundary	q_b	0.8471	mW m^{-2}
Chondritic heating		5×10^{-12}	W kg^{-1}
Empirical parameter for Andrade model[b]	α_A	0.33	
Empirical parameter for Andrade model[b]	ζ	1	
Current eccentricity	e_0	0.0045	
Orbital period	T_O	1.37	day
Spin period	T_R	1.37	day
Ocean width	Δ	120,180,360	deg
Temperature contrast	ΔT	200	K
Temperature at the surface	T_S	73	K

[a] Physical parameters estimated at melting temperature from Hobbs (1974).
[b] From Castillo-Rogez et al. (2011).

50 convection time steps following the procedure described in detail in Běhounková et al. (2010), and a convergence parameter equal to 10^{-8} is used.

2.2. Rheology

The viscous creep of ice is known to depend on various parameters including temperature, strain rate and grain size (e.g. Goldsby and Kohlstedt, 2001; Durham et al., 2001). Here, we have extended the rheological description used in Běhounková et al. (2012) in order to take into account a more realistic rheology including dislocation creep, grain-size-sensitive creep (gss), which may occur via a combination of grain boundary sliding (gbs) and basal sliding (bs), and diffusion creep. The total strain rate of ice I then results from the combination of strain rate associated with each creep mechanism:

$$\dot{\varepsilon} = \dot{\varepsilon}_{\mathrm{diff}} + \dot{\varepsilon}_{\mathrm{disl}} + \left(\frac{1}{\dot{\varepsilon}_{\mathrm{gbs}}} + \frac{1}{\dot{\varepsilon}_{\mathrm{bs}}}\right)^{-1}. \quad (1)$$

The strain rate $\dot{\varepsilon}_{\bullet}$ for each creep mechanism is described by

$$\dot{\varepsilon}_{\bullet} = A\frac{\sigma^n}{d^m}\exp\left(\frac{Q^*}{RT}\right), \quad (2)$$

where σ is stress, T temperature, d grain size, R gas constant and A, n, m, Q^* are parameters inherent to a given deformation mechanism. To compute the composite viscosity, we use the parameters provided by Goldsby and Kohlstedt (2001) (summarized in Table 2), and we employ an explicit strain rate-dependent rheology (see e.g. Barr and Pappalardo, 2005). Except for dislocation creep, the other mechanisms depend on grain size. Depending on temperature, grain size and strain rate, each of these mechanisms may become a dominant creep mechanism. Fig. 1a shows that, for the strain rate expected in a convective ice shell on Enceladus (for typical values of $\sim 10^{-12}$ s^{-1}) and a fixed grain size of 1 mm, diffusion creep is the prevailing mechanism in most of the convective region. Grain-size-sensitive and dislocation creeps become dominant only in the cold thermal boundary layer and in the conductive lid. As indicated above, in the case of the viscous convective flow, a viscosity cut-off corresponding to a maximum viscosity contrast of 10^8 is prescribed for numerical reasons (see black line in Fig. 1a).

For sake of simplicity, we consider here constant grain size values in the whole domain. In reality, the grain size is expected to evolve as a function of temperature and strain rate owing to normal grain growth and dynamical recrystallization (e.g. Montagnat and Duval, 2000; Durand et al., 2006; Barr and McKinnon, 2007b). In order to better understand how grain size affects the onset of convection in tidally-heated layers, we chose here to consider the grain size as a fixed parameter. The effect of grain size evolution will be addressed in a future study.

Laboratory experiments indicate that the anelastic response also depends on a variety of parameters including temperature, stress, grain size, dislocation density, water content, salinity, porosity etc. (e.g. Tatibouet et al., 1986; Cole, 1995; McCarthy and Castillo-Rogez, 2013). A complex rheological law is thus needed to describe correctly the anelastic response. However, laboratory experiments performed at frequencies representative of tidal frequency (10^{-6}–10^{-5} s^{-1}) are still lacking. The incompressible Maxwell rheology is commonly used owing to its simplicity, as it is described by only two parameters, the viscosity η and the elastic shear modulus μ. The Maxwell rheology approximates correctly the dissipative processes for forcing periods around or above the Maxwell time $\tau_{\mathrm{M}} = \eta/\mu$. Nevertheless, the Maxwell rheology underestimates the dissipation rate for forcing periods shorter than the Maxwell time (e.g. Sotin et al., 2009; Efroimsky, 2012). In the case of Enceladus with a forcing period of 1.37 day, the tidal heating is considerably underestimated for viscosities larger than 10^{15} Pa s. The Andrade model is suggested to provide a better description of the anelastic response (Castillo-Rogez et al., 2011; McCarthy and Castillo-Rogez, 2013). In addition to the Maxwell time τ_{M}, it relies on two additional empirical parameters α_{A} and $\zeta = \frac{\tau_{\mathrm{A}}}{\tau_{\mathrm{M}}}$, where τ_{A} is the Andrade (anelastic) time (see e.g. Efroimsky, 2012).

Table 2
Rheological parameter, see Goldsby and Kohlstedt (2001).

	n	m	T K	A m^m Pa^{-n} s^{-1}	Q^* kJ/mol	T K	A m^m Pa^{-n} s^{-1}	Q^* kJ/mol
Diffusion creep	1	2	–	3.3×10^{-10}	60	–	–	–
Basal-slip accommodated GBS	2.4	0	–	2.2×10^{-7}	60	–	–	–
GBS-accommodated basal slip	1.8	1.4	<255	6.2×10^{-14}	49	>255	4.8×10^{15}	192
Dislocation creep	4.0	0	<258	4.0×10^{-19}	60	>258	6.0×10^{4}	180

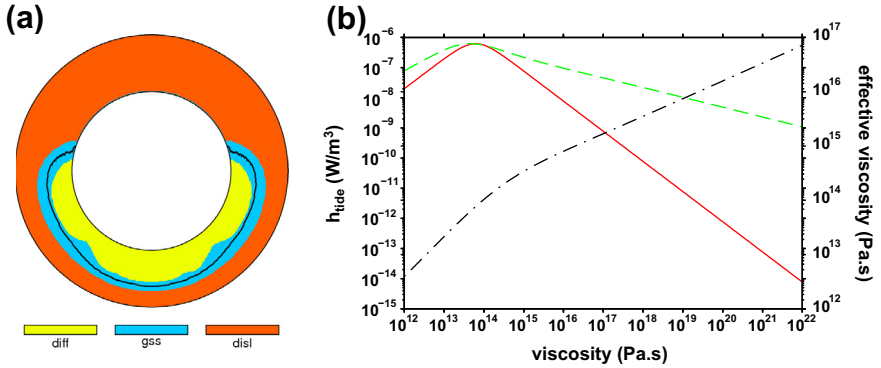

Fig. 1. (a) An example of prevailing deformation mechanism for $\Delta = 180°$, $3e_0$ and $d = 1$ mm; black line denotes the viscosity cut-off used for the viscous flow. (b) Tidal heating rate as a function of the viscosity for tidal strain rate 10^{-10} s^{-1}; solid red line – tidal heating for a Maxwell body, dashed green line – tidal heating for the Andrade-like rheology using the effective tidal viscosity. Effective tidal viscosity as a function of the viscosity (dash-dotted black line). (For interpretation of the references to color in this figure legend, the reader is referred to the web version of this article.)

In the case of Enceladus, strong lateral variations of internal temperature are expected, and thus including lateral variations of viscosity within the viscoelastic model is an essential issue. In order to include the lateral variations, the anelastic response has to be solved in the time domain which is challenging in the case of the Andrade model. We thus mimic the Andrade rheology using a Maxwell-like formalism where we define an effective tidal viscosity $\hat{\eta}$ in order to reproduce the dissipation rate expected with an Andrade model. The effective viscosity is calculated as follows:

$$\tan\delta_A(\eta) \equiv \tan\delta_M(\hat{\eta}), \tag{3}$$

where δ_A and δ_M are the phase lags for the Andrade and Maxwell models, respectively. Using the theoretical relationships for $\tan\delta_A$ and $\tan\delta_M$ (see e.g. Efroimsky, 2012), this leads to the following expression of the effective viscosity $\hat{\eta}$ for a given angular frequency ω:

$$\hat{\eta} = \frac{1+\left(\frac{\mu}{\omega\zeta\eta}\right)^{\alpha_A}\left(\Gamma(\alpha_A+1)\cos\frac{\alpha_A\pi}{2}\right)}{\frac{1}{\eta}+\frac{1}{\eta^{\alpha_A}}\left(\frac{\mu}{\omega\zeta}\right)^{\alpha_A-1}\left(\Gamma(\alpha_A+1)\sin\frac{\alpha_A\pi}{2}\right)}. \tag{4}$$

The effective viscosity $\hat{\eta}$ as a function of the convective viscosity η is shown in Fig. 1b (black dash-dotted line). Owing to this correction, the decrease as a function of viscosity is much less pronounced in the Andrade-like model described above than in the classical Maxwell model, which is more compatible with available experimental data (cf. Fig. 1b, green and red lines).

3. Onset of convection in a heterogeneously heated layer

The onset of convection within a variable-viscosity fluid system heated from below and/or from within has been studied extensively (e.g. Stengel et al., 1982; Davaille and Jaupart, 1994; and in a spherical geometry by Běhounková and Choblet (2009)) and applied to icy satellites (e.g. Barr and Pappalardo, 2005). While a classical approach for isoviscous fluids can be based on linear stability analysis (e.g. Chandrasekhar, 1961), it has been noted that a Newtonian variable-viscosity fluid presents a range below the critical Rayleigh number where some finite-amplitude perturbations do not decay (cf. e.g. Busse, 1967). In the case of a power-law viscosity, fluids are stable to any infinitesimal perturbation so that perturbations have to be finite in order to initiate convection: Solomatov and Barr (2006) have investigated the absolute minimum critical Rayleigh number for such a fluid, below which all perturbations decay independently of the amplitude. Solomatov and Barr (2007) studied what should be the nature of a perturbation to trigger convection for a given Rayleigh number. A first attempt to precisely characterize subcritical convection for a temperature-dependent viscosity fluid is proposed by Solomatov (2012).

Given this complexity, Barr and McKinnon (2007a) first established from scaling relationships how the onset of convection in the icy shell of Enceladus likely involves the interplay of various creep mechanisms and can be triggered by a temperature anomaly caused by tidal heating. We follow here this work through our numerical experiments where thermal convection and tidal dissipation are fully coupled. The present model for Enceladus includes two specific aspects influencing the onset of convection: a composite flow law is considered for ice that includes both Newtonian and power-law mechanisms (and thus combines distinct behaviors for the stability of thermal perturbations), and heterogeneous heating. Note that one component of the latter is associated with the specific boundary conditions (presence of a liquid ocean beneath the ice shell in the south polar region) so that a large-scale heating anomaly will persist there regardless of the initiation of convection. Thermal perturbations associated with this contribution therefore cannot decay. A second contribution is associated with the feedback between tidal heating and convective planform through the temperature dependence of viscoelastic dissipation and will also have an effect on the occurrence of convection. These heating heterogeneities are potentially located in the rheological sublayer beneath the stagnant lid which has been demonstrated to be the most effective location for the initiation of convection (Solomatov and Barr, 2007).

In the following we will distinguish cases where a large-scale lateral flow results from the non-decaying heating heterogeneity above the liquid ocean (cf. Fig. 2c) and cases where viscosity is small enough for small-scale convective instabilities to develop in the same region (cf. Fig. 2a and b). The term "convective cases" only applies to the latter although large-scale flow with small, but finite velocity is observed in the former cases (compare Fig. 2d,e and f). A simple criterion to discriminate among the two groups is obtained from the respective contributions of advection and diffusion to radial heat transfer in the region above the liquid ocean: (i) a "convecting case" corresponds to a system where radial advective heat transfer is predominant in a sublayer located between the cold boundary layer including the stagnant lid and a thin basal hot boundary layer. Within the thermal boundary layers (by definition) conductive heat transfer prevails over the advective heat transfer; and (ii) a "non-convecting case" corresponds to a system where conduction is at every depth the main mechanism for radial heat transfer.

4. Critical grain size for the onset of convection

The occurrence of convection is primarily controlled by the grain size and the tidal heating rate. Since diffusion creep, which is strongly grain-size dependent, is the prevailing mechanism in most of the convective ice shell, the minimum viscosity within the domain and the onset of convection are thus controlled by the grain size. The presence of internal heating favors the onset of convection as it increases temperature anomalies in growing convective instabilities, thus reducing locally the viscosity and increasing the buoyancy. As a consequence, as illustrated in Fig. 3, the critical grain size for the onset of convection increases with increasing heating rate.

In the absence of tidal dissipation, our simulations show that convection initiates for grain size values lower than or equal to 0.5 mm. This is consistent with the typical value derived by Barr and McKinnon (2007a) using scaling laws. Convective instabilities develop uniformly above the entire internal water reservoir (see Fig. 2a). The increase of convective velocity results in a rapid increase of the power extracted from the ocean (P_b, Fig. 2d).

If tidal heating is introduced, the onset of convection is favored by tidal dissipation, and therefore the onset of convection is initiated for larger grain size ($\sim$1 mm) in the polar region above the water reservoir where tidal dissipation is maximal (see Fig. 2b). We observe an increase of the dissipated power, P_{tide}, which counterbalances the enhanced efficiency of heat transfer due to the development of convection. As a consequence, the bottom power (P_b) extracted from the ocean is reduced compared to the initial conductive case.

The extension of the convective region is controlled by the dissipation rate, the dissipation pattern and the grain size. For the results displayed in Fig. 2b with d = 1 mm, no convection develops in the equatorial region as the amplitude of tidal heating is too small for convection to be triggered there. For a grain size of 0.6 mm, the convection is eventually observed at low latitudes even for low eccentricity values ($e = e_0$) and for $\Delta = 180°$ when the maximum tidal heating is only $\sim 0.2 \times 10^{-6}$ W m^{-3}. For grain size of 1 mm and $\Delta = 180°$, convection is observed in the equatorial region for

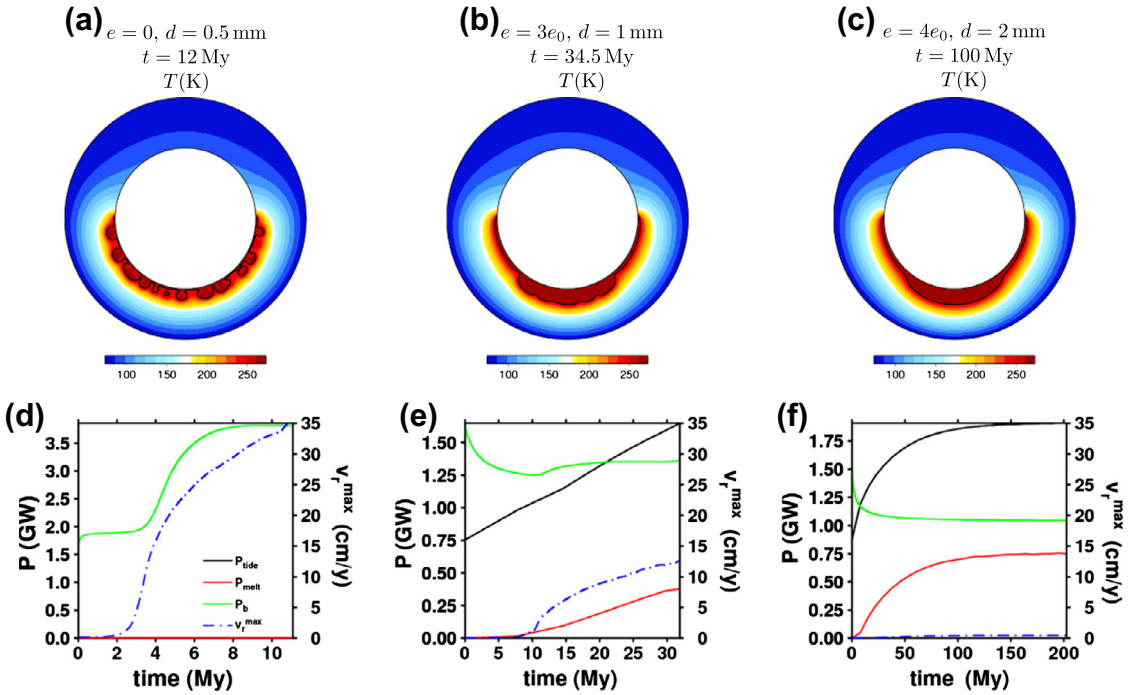

Fig. 2. Top row – temperature patterns at the onset of convection and bottom row – evolution of global tidal heating P_{tide} (black solid line), energy loss of the ocean P_b (green solid line), latent heating P_{melt} (red solid line) and maximum radial velocity (blue, dash-dotted line) for (a and d) $\Delta = 180°$, grain size 0.5 mm without any tidal heating, (b and e) $\Delta = 180°$, grain size 1 mm and $e = 3e_0$ where the convection is triggered by the tidal dissipation; (c and f) the temperature pattern for non-convecting case $\Delta = 180°$, $e = 4e_0$ and grain size 2 mm. (For interpretation of the references to color in this figure legend, the reader is referred to the web version of this article.)

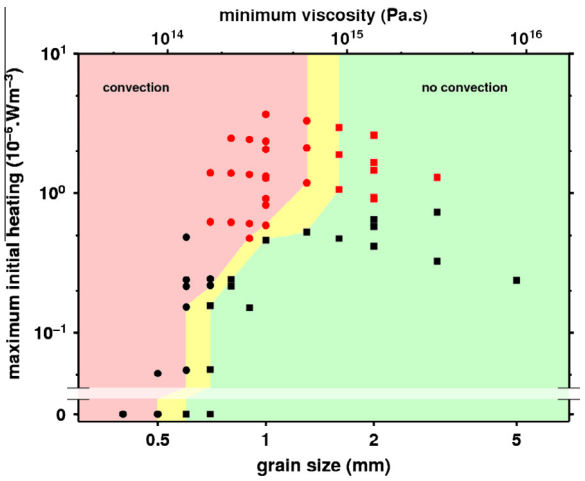

Fig. 3. Phase diagram depending on the grain size and maximum initial heating rate, circles – convecting cases, squares – non-convecting cases, black color – no melt is present, red color – melt is present. (For interpretation of the references to color in this figure legend, the reader is referred to the web version of this article.)

eccentricity higher than or equal to $4e_0$ corresponding to a maximum initial heating rate of $\sim 2 \times 10^{-6}$ W m^{-3}.

The minimum grain size needed to initiate convection naturally increases with the heating rate. The critical grain size for the onset of convection increases only faintly for heating rates below 0.2×10^{-6} W m^{-3}. The increase is more pronounced for heating rate values between 0.2 and 1×10^{-6} W m^{-3}. Above 1×10^{-6} W m^{-3}, we do not observe any further increase of the critical grain size. Moreover, we observe the occurrence of melting within the ice shell for tidal heating rates typically exceeding $0.5–0.9 \times 10^{-6}$ W m^{-3}. The transition between cases with and without melting depends slightly on the grain size (Fig. 3). The occurrence of melting may explain why the critical grain size stops increasing for heating rates above 10^{-6} W m^{-3}, as it limits any further increase of the internal temperature.

The width of the internal water reservoir does not influence directly the onset of convection above the internal water reservoir. For simulations with no tidal heating, the critical grain size remains the same whatever the ocean width. Nevertheless, as the amount of tidal heating is strongly influenced by the ocean width (see also Běhounková et al., 2012), it has a significant influence on the onset of convection for simulations with tidal heating. Considerably higher eccentricity has to be considered for cases with a small internal ocean, especially for $\Delta \leqslant 120°$, than for cases with $\Delta \geqslant 180°$ in order to observe similar tidal heating production and to trigger convection. For example, if grain size $d = 1$ mm is considered, the eccentricity needed to trigger convection is $4e_0$ for $\Delta = 120°$, while it is only $2e_0$ for $\Delta \geqslant 180°$.

5. Discussion and conclusions

As shown by our simulations, the criterion for the occurrence of convection depends on the heating rate and hence on the eccentricity and the width of the internal ocean. Therefore, it is expected that Enceladus may switch from conductive to convective states depending on its orbital configuration. We showed in a previous study (Běhounková et al., 2012) that Enceladus can remain dissipative and active only during relatively short periods of time (<10 Myr). After an active period, the heating rate may rapidly decrease below 10^{-7} W m^{-3}, owing to eccentricity damping. According to the diagram in Fig. 3, for such low heating rates, convection is possible only for grain sizes smaller than 0.5 mm. Such small grain sizes might be preserved via grain boundary pinning only if the ice contains a significant fraction of impurities (e.g. Barr and McKinnon, 2007a,b). The presence of rock, salt or clathrate particles at the grain boundaries may indeed limit the normal grain growth as has been shown in terrestrial polar ice cores (e.g. Alley et al., 1986). However, following the pinning model of Durand

et al. (2006), a volume fraction of at least 5–15% of 0.1-mm secondary phase particles is required to limit the ice grain size to 0.5 mm. Such elevated particle concentrations seem a priori incompatible with the composition of Enceladus's surface and plume particles, which are dominated by water ice (Brown et al., 2006; Postberg et al., 2011). It seems therefore unlikely that grain sizes smaller than 0.5 mm are present within Enceladus's ice layer, and therefore the ice shell should not be convective if the heating rate is smaller than roughly $1–2 \times 10^{-7}$ W m^{-3}.

During periods of low dissipation, the orbital eccentricity is expected to progressively increase due to tidal dissipation within Saturn, on timescales of ~100 Myr (e.g. Běhounková et al., 2012). Depending on the ocean width, the heating rate may become larger than 5×10^{-7} W m^{-3} when the eccentricity reaches values two to five times the present-day value. The onset of convection thus becomes possible for a maximum grain size of about 1.5 mm. Pinning effects may limit the grain size to such a value if the ice contains roughly 0.5–2% of 0.1-mm secondary phase particles (which is more reasonable that the 5–15% required for grain sizes of 0.5 mm). Dynamic recrystallization may also counteract normal grain growth (De Bresser et al., 1998; Montagnat and Duval, 2000; Barr and McKinnon, 2007b), but only if a significant fraction of the strain rate is due to dislocation creep. As shown in Fig. 1a, diffusion creep is the dominant deformation process for grain sizes of about 1 mm, and the dislocation and GSS creeps do not produce strain rates larger than $\sim 10^{-15}$ s^{-1}. In such conditions, no significant dynamic recrystallization is expected due to convection alone.

For heating rates larger than $5–9 \times 10^{-7}$ W m^{-3}, we systematically observe the occurrence of melting in our simulations, whatever the grain size and both for convecting and non-convecting cases (Fig. 3). A first consequence of melting is the generation of liquid pores along the grain boundaries, possibly reducing the driving force for grain coarsening by transient pinning (e.g. Alley et al., 1986). A more important consequence is the change of volume due to ice melting, which has been shown to produce a large stress accumulation in the ice shell (Běhounková et al., 2012). As mentioned in this latter study, stress concentration in the south polar region may result in the rupture of the ice lithosphere, possibly triggering the observed surface activity. This stress enhancement would also favor stress-dependent dislocation and GSS creeps, and therefore it may reduce the average grain size by dynamic recrystallization. Due to this reduction effect, it is possible, even for initially non-convecting cases ($d > 1.5$ mm), to switch to a convective state once melting occurs.

Both impurities and tidally-induced melting may play a key role on the onset of convection in Enceladus's ice shell, by controlling grain growth and dynamic recrystallization. In our simulations, the presence of impurities and interstitial melts are neglected: a pure water system is considered, and any produced melt is instantaneously extracted from the convective layer (see Section 2.1). In reality, a non-negligible fraction of impurities, such as salts, and brine pockets may be present. A melt fraction as small as 1–2% would be sufficient to annihilate the positive buoyancy of ice hot plumes (Tobie et al., 2003). The presence of impurities, which may reduce the melting point, as well as the retention of interstitial melts would make the convective solution much more complex, by influencing the density and rheological properties of the mixture. A precise investigation of all these aspects would be needed to thoroughly understand the combined role of grain size evolution, melt generation and transport and how they affect the coupled thermal and orbital evolution of Enceladus.

Acknowledgments

The comments of two anonymous reviewers are gratefully acknowledged. The authors thank Craig Bina for his comments and English corrections. The research leading to these results has received funding from the European Research Council under the European Community's Seventh Framework Program (FP7/2007–2013 Grant Agreement No. 259285), from the Czech Science Foundation Project No. P210/10/P306, from the Research Program MSM0021620860 of the Ministry of Education of the Czech Republic and from the Czech–French Program Barrande No. MEB021129. The computations were carried out using CCIPL and CINES computational facilities (France).

References

Alley, R.B., Perepezko, J.H., Bentley, C.R., 1986. Grain growth in polar ice: I. Theory. J. Glaciol. 32, 415–424.
Barr, A., McKinnon, W., 2007a. Convection in Enceladus ice shell: Conditions for initiation. Geophys. Res. Lett. 34, L09202.
Barr, A., McKinnon, W., 2007b. Convection in ice I shells and mantles with self-consistent grain size. J. Geophys. Res. 112, 2012.
Barr, A., Pappalardo, R., 2005. Onset of convection in the icy Galilean satellites: Influence of rheology. J. Geophys. Res. 110, E12005.
Běhounková, M., Choblet, G., 2009. Onset of convection in a basally heated spherical shell, application to planets. Phys. Earth Planet. Int. 176, 157–173.
Běhounková, M., Tobie, G., Choblet, G., Čadek, O., 2010. Coupling mantle convection and tidal dissipation: Applications to Enceladus and Earth-like planets. J. Geophys. Res. 115, E09011.
Běhounková, M., Tobie, G., Choblet, G., Čadek, O., 2012. Tidally-induced melting events as the origin of south-pole activity on Enceladus. Icarus 219, 655–664.
Brown, R.H. et al., 2006. Composition and physical properties of Enceladus' surface. Science 311, 1425–1428.
Busse, F.H., 1967. The stability of finite amplitude cellular convection and its relation to an extremum principle. J. Fluid Mech. 30, 625–649.
Castillo-Rogez, J.C., Efroimsky, M., Lainey, V., 2011. The tidal history of Iapetus: Spin dynamics in the light of a refined dissipation model. J. Geophys. Res. (Planets) 116, E09008.
Chandrasekhar, S., 1961. Hydrodynamic and Hydromagnetic Stability. Oxford University Press.
Choblet, G., 2005. Modelling thermal convection with large viscosity gradients in one block of the 'cubed sphere'. J. Comput. Phys. 205, 269–291.
Choblet, G., Čadek, O., Couturier, F., Dumoulin, C., 2007. ŒDIPUS: A new tool to study the dynamics of planetary interiors. Geophys. J. Int. 170, 9–30.
Cole, D., 1995. A model for the anelastic straining of saline ice subjected to cyclic loading. Phys. Mag. A 72, 231–248.
Davaille, A., Jaupart, C., 1994. Onset of thermal convection in fluids with temperature-dependent viscosity—applications to the oceanic mantle. J. Geophys. Res. 99, 19853–19866.
De Bresser, J.H.P., Peach, C.J., Reijs, J.P.J., Spiers, C.J., 1998. On dynamic recrystallization during solid state flow: Effects of stress and temperature. Geophys. Res. Lett. 25, 3457–3460.
Durand, G. et al., 2006. Effect of impurities on grain growth in cold ice sheets. J. Geophys. Res. 111, F01015.
Durham, W.B., Stern, L.A., Kirby, S.H., 2001. Rheology of ice I at low stress and elevated confining pressure. J. Geophys. Res. 106, 11031–11042.
Efroimsky, M., 2012. Tidal dissipation compared to seismic dissipation: In small bodies, Earths, and super-Earths. Astrophys. J. 746, 150.
Goldsby, D., Kohlstedt, D., 2001. Superplastic deformation of ice: Experimental observations. J. Geophys. Res. 106, 11017–11030.
Han, L., Tobie, G., Showman, A.P., 2012. The impact of a weak south pole on thermal convection in Enceladus' ice shell. Icarus 218, 320–330.
Hobbs, P.V., 1974. Ice Physics. Clanderon, Oxford, England.
Howett, C.J.A., Spencer, J.R., Pearl, J., Segura, M., 2011. High heat flow from Enceladus' south polar region measured using 10–600 cm^{-1} Cassini/CIRS data. J. Geophys. Res. 116, E03003.
Kalousová, K., Souček, O., Tobie, G., Choblet, G., Čadek, O., 2013. Water production and transport in Europa's ice shell. Icarus, submitted for publication.
McCarthy, C., Castillo-Rogez, J.C., 2013. Planetary ices: Attenuation properties. In: Gudipati, M., Castillo-Rogez, J.C. (Eds.), The Science of Solar System Ices. Springer.
Meyer, J., Wisdom, J., 2007. Tidal heating in Enceladus. Icarus 188, 535–539.
Mitri, G., Showman, A.P., 2008a. A model for the temperature-dependence of tidal dissipation in convective plumes on icy satellites: Implications for Europa and Enceladus. Icarus 195, 758–764.
Mitri, G., Showman, A.P., 2008b. Thermal convection in ice-I shells of Titan and Enceladus. Icarus 193, 387–396.
Montagnat, M., Duval, P., 2000. Rate controlling processes in the creep of polar ice, influence of grain boundary migration associated with recrystallization. Earth Planet. Sci. Lett. 183, 179–186.
Nimmo, F., Pappalardo, R.T., 2006. Diapir-induced reorientation of Saturn's moon Enceladus. Nature 441, 614–616.
Nimmo, F., Spencer, J.R., Pappalardo, R.T., Mullen, M.E., 2007. Shear heating as the origin of the plumes and heat flux on Enceladus. Nature 447, 289–291.
Porco, C. et al., 2006. Cassini observes the active south pole of Enceladus. Science 311, 1393–1401.

Postberg, F., Schmidt, J., Hillier, J., Kempf, S., Srama, R., 2011. A salt-water reservoir as the source of a compositionally stratified plume on Enceladus. Nature 474, 620–622.
Roberts, J., Nimmo, F., 2008. Tidal heating and the long-term stability of a subsurface ocean on Enceladus. Icarus 194, 675–689.
Schubert, G., Anderson, J.D., Travis, B.J., Palguta, J., 2007. Enceladus: Present internal structure and differentiation by early and long-term radiogenic heating. Icarus 188, 345–355.
Solomatov, V.S., 2012. Localized subcritical convective cells in temperature-dependent viscosity fluids. Phys. Earth Planet. Int. 200, 63–71.
Solomatov, V., Barr, A., 2006. Onset of convection in fluids with strongly temperature-dependent, power-law viscosity. Phys. Earth Planet. Int. 155, 140–145.
Solomatov, V., Barr, A., 2007. Onset of convection in fluids with strongly temperature-dependent, power-law viscosity 2. Dependence on the initial perturbation. Phys. Earth Planet. Int. 165, 1–13.
Sotin, C., Tobie, G., Wahr, J., McKinnon, W.B., 2009. Tides and tidal heating on Europa. In: Pappalardo, McKinnon, K. (Eds.), Europa. The University of Arizona Press, pp. 85–118.
Spencer, J. et al., 2006. Cassini encounters Enceladus: Background and the discovery of a south polar hot spot. Science 311, 1401–1405.
Spencer, J.R. et al., 2009. Enceladus: An Active Cryovolcanic Satellite. p. 683.
Stegman, D.R., Freeman, J., May, D.A., 2009. Origin of ice diapirism, true polar wander, subsurface ocean, and tiger stripes of Enceladus driven by compositional convection. Icarus 202, 669–680.
Stengel, K., Oliver, D., Booker, J., 1982. Onset of convection in a variable viscosity fluid. J. Fluid Mech. 120, 411–431.
Tatibouet, J., Perez, J., Vassoille, R., 1986. Study of grain-boundaries in ice by internal friction measurements. J. Phys. 48, 197–203.
Tobie, G., Choblet, G., Sotin, C., 2003. Tidally heated convection: Constraints on Europas ice shell thickness. J. Geophys. Res. 108, 5124. http://dx.doi.org/10.1029/2003JE002099.
Tobie, G., Čadek, O., Sotin, C., 2008. Solid tidal friction above a liquid water reservoir as the origin of the south pole hotspot on Enceladus. Icarus 196, 642–652.
Zhang, K., Nimmo, F., 2009. Recent orbital evolution and the internal structures of Enceladus and Dione. Icarus 204, 597–609.